

On the Relationship between Graphical Gaussian Processes and Functional Gaussian Graphical Models

Debangana Dey¹, Abhirup Datta², and Sudipto Banerjee³

¹Johns Hopkins Bloomberg School of Public Health,, 615 N Wolfe St,
Baltimore, MD 21205, USA

²Department of Biostatistics, University of California Los Angeles

September 15, 2022

Abstract

Multivariate functional or spatial data are commonly analysed using multivariate Gaussian processes (GP). Two recent approaches extend Gaussian graphical models (GGM) to multivariate Gaussian processes with each node representing an entire GP on a continuous domain and edges representing process-level conditional independence. The functional GGM uses a basis function expansion for a multivariate process and models the vector coefficients of the basis functions using GGM. Graphical GP directly constructs valid multivariate covariance functions by *stitching* univariate GPs, while exactly conforming to a given graphical model and retaining marginal properties. We bridge the two seemingly disconnected paradigms by proving that any partially separable functional GGM with a specific covariance selection model is a graphical GP. We also show that the finite term truncation of functional GGM is equivalent to stitching using a low-rank GP, which are known to oversmooth marginal distributions. The theoretical connections help design new algorithms for functional data that exactly conforms to a given inter-variable graph and also retains marginal distributions.

Keywords: Gaussian Processes; Multivariate analysis; Functional data; Graphical models; Spatial data

1 Introduction

Gaussian graphical models (GGM) have been extensively used to represent sparsity structures emerging from conditional independence relations among a collection of Gaussian random variables. The graph determines the zeroes of the precision (inverse-covariance) matrix of multivariate observations. Of key interest is conducting multivariate analysis when the variables conform to a given graph. Covariance selection (Dempster, 1972) offers a seminal result to answer this specific question. If the graph is unknown, then classical approaches, such as the graphical Lasso, estimate a sparse precision matrix through L-1 regularization (Friedman et al., 2008; Meinshausen & Bühlmann, 2006). Bayesian alternatives employ Markov chain Monte Carlo (MCMC) algorithms with a conjugate hyper-inverse Wishart prior for estimating both the graph and the precision matrix (Dobra et al., 2011; Roverato, 2002; Carvalho et al., 2007).

Graphical Gaussian models are customarily applied to multivariate data sets, where the data units, i.e., the nodes of the graph, are scalar- or vector-valued. Data sets often comprise multiple functions or processes that conceptually exist in continuum over a domain (e.g., over space or time). Examples of such functional data include physical activity or heart rate continuously measured from actigraph monitors (wearables), EEG/fMRI signals from different brain regions (neuroimaging), multiple-gene expressions from cells distributed over a tissue (spatial transcriptomics), population counts of multiple biological species over a region (ecology) and multiple pollutants measured from environmental monitoring stations (environmental sciences).

Multivariate functional data is often modelled using a latent multivariate stochastic process, such as a multivariate Gaussian process (GP) (Wackernagel (2013); Banerjee et al. (2014); Cressie & Wikle (2011); Qiao et al. (2019)). Hence, it is natural to seek extensions of graphical models for multivariate functional data, where each node represents an entire function or stochastic process. Two recent approaches have extended the GGM to represent conditional dependencies among multivariate stochastic processes on continuous domains: (i) functional GGM (FGGM); and (ii) graphical Gaussian Process (GGP). The former relies on a multivariate Karhounen-Loève basis expansion and imposes sparsity on the precision matrices of the Gaussian coefficient vectors via penalised estimation (Zapata et al., 2021; Zhu et al., 2016).

Functional GGMs have been primarily used for functional data analysis, which customarily uses basis function representations but has also been applied to spatial data (Krock et al., 2021). The method requires replicated data as it estimates the unknown graph.

Graphical GP (Dey et al., 2021) focuses on multivariate spatial analysis and proposes a multivariate GP covariance function that exactly conforms to a prespecified graph. This new class of multivariate GPs is essentially an extension of Dempster’s covariance selection to infinite-dimensional settings. Given a non-graphical multivariate covariance function, it obtains the optimal graphical covariance function with process-level conditional independence as specified by an undirected graph. A graphical GP is constructed by an algorithm called *stitching*, which ensures scalable likelihood-based analysis of *highly multivariate* spatial data with a large number of outcome variables by leveraging the sparsity of the graph. Graphical GP retains marginal and edge-specific covariances from a parametric multivariate covariance function, thereby facilitating interpretation of the spatial attributes of each process via inference on the parameters, which is often the primary inferential objective in spatial analysis. Unlike the functional GGM, graphical GP does not need replicate data which is unavailable in many spatial applications.

Our current contribution can be summarised as follows. Functional GGM and graphical GP are apparently complementary methods for introducing graphical models in multivariate GP. The former relies on basis function expansions and is typically used for functional data. Graphical GP focuses on spatial data and directly uses covariance functions. We bridge these two seemingly disconnected paradigms. We formally establish that the class of *partially separable* functional GGM (Zapata et al., 2021) with a specific model for the covariance matrices of the coefficients is equivalent to a graphical GP. Furthermore, using Nyström’s method, we relate the stitching algorithm for construction of graphical GP to a finite-term truncation of basis functions used in functional GGM. The theoretical connections made here have important implications for multivariate functional analysis. When the graph is known (e.g. existing brain-region networks, phylogenetic trees etc.), current estimation strategies for functional GGM cannot use or respect knowledge of the graph. We leverage the equivalence between functional GGM and graphical GP to design two algorithms for analysis of multivariate functional data that exactly preserve the given functional conditional independence relationships.

2 The two paradigms

2.1 Functional Gaussian graphical models

Let $w(\cdot) = (w_1(\cdot), \dots, w_q(\cdot))^T$ be a $q \times 1$ GP over a continuous domain \mathcal{D} with node j representing the univariate process $w_j(\cdot)$ for $j = 1, 2, \dots, q$. For a set of variables $\mathcal{V} = \{1, \dots, q\}$, two univariate GPs $w_i(\cdot)$ and $w_j(\cdot)$ are conditionally independent, given the remaining processes $\{w_k(\cdot) \mid k \in \mathcal{V} \setminus \{i, j\}\}$ if $\text{Cov}(\epsilon_{iB}(s), \epsilon_{jB}(s')) = 0$ for all $s, s' \in \mathcal{D}$ and $B = \mathcal{V} \setminus \{i, j\}$, where $\epsilon_{kB}(s) = w_k(s) - \mathbb{E}[w_k(s) \mid \sigma(\{w_j(s') : j \in B, s' \in \mathcal{D}\})]$ (Dey et al., 2021). Here $\sigma(\cdot)$ is the σ -algebra generated by its argument.

Functional GGM introduces this process-level conditional independence through the precision matrices of coefficient vectors in its basis expansion. Letting ϕ_{jl} be the set of orthonormal basis functions in the domain \mathcal{D} , the process is represented as $w_j(s) = \sum_{l=1}^{\infty} \theta_{jl} \phi_{jl}(s)$. Zhu et al. (2016) shows that modelling the coefficients θ_{jl} to be Gaussian and assuming a sparsity structure between the discrete multivariate GP $\theta^{(j)} = \{\theta_{jl} : l = 1, \dots, \infty\}$ imposes the corresponding process-level conditional independence among the component processes of $w(\cdot)$. In practice, they truncate the expansion of $\theta^{(j)}(\cdot)$ to m_j terms and fit a GGM on the $M = \sum_{j=1}^q m_j$ dimensional vector of coefficients. The approach involves inversion of an $M \times M$ matrix, thereby requiring $O(M^3)$ floating point operations (FLOPs) or $O(q^3 m^3)$ FLOPs when $m_j = m$ for all j . The computational expense being cubic in the number of basis functions m , prohibits large values m which, in turn, can restrict the richness of the function class.

The functional GGM in Zapata et al. (2021) and Krock et al. (2021) introduce two further assumptions: (a) a common orthonormal basis function, i.e, $\phi_{jl} = \phi_l$ for all $j = 1, \dots, q$; and (b) the coefficients corresponding to different basis functions are independent, i.e, θ_j and θ_k are independent, where $\theta_j = (\theta_{1j}, \dots, \theta_{qj})$. Due to the separability in the joint covariance structure of basis coefficients, they are formally termed as *partial separable* processes (Zapata et al., 2021). Their practical implementation truncates the basis function expansion to m terms and uses graphical Lasso on the estimated covariance of the coefficient vectors to induce sparsity. This partial separable structure only needs m inversions of $q \times q$ matrices and considerably reduces computational complexity to $O(mq^3)$. All functional GGM (i) need replicate observa-

tions to estimate basis functions and sample covariances, and cannot be applied to spatial data without replicates; (ii) do not retain the marginal processes as we need to truncate the basis functions.

2.2 Graphical Gaussian Processes

Spatial data often lack replicates and is, therefore, modelled using GPs with parametric covariance functions. This contrasts the functional data setup with replicates, which enables functional GGM to estimate a non-parameteric covariance function. The Matérn family of covariances (Stein, 1999) are popular in spatial analysis because their parameters can be interpreted as the variance, spatial smoothness and range of the process. Dey et al. (2021) introduced graphical Gaussian process (GGP) models attuned to analyse highly multivariate spatial data. These are specified through multivariate covariance functions that exactly encode an inter-variable graphical model. Theorem 1 in Dey et al. (2021) asserts that given a non-graphical stationary multivariate GP and an inter-variable graph, the unique and optimal graphical GP approximating the original GP (in terms of integrated spectral Kullback-Leibler divergence) will retain the univariate marginal distributions and edge-specific cross-covariances from the original GP. This result generalises covariance selection (Dempster, 1972) from finite-dimensional covariance matrices to infinite-dimensional covariance operators. We denote this optimal graphical GP derived from the original covariance function C and a graph \mathcal{G} as $GGP(C, \mathcal{G})$.

Definition 2.1. $w(\cdot) \sim GGP(C, \mathcal{G})$ is a $q \times 1$ graphical GP on \mathcal{D} given a valid $q \times q$ cross-covariance function $C = (C_{ij})$ on $\mathcal{D} \subseteq \mathbb{R}^d$ and a graph $\mathcal{G} = (\mathcal{V}, E)$, such that $w_j(\cdot) \sim GP(0, C_{jj})$ for all $1 \leq j \leq q$, $Cov(w_i(s), w_j(t)) = C_{ij}(s, t)$ for all $(i, j) \in E$ and $s, t \in \mathcal{D}$, and $w_i(\cdot) \perp w_j(\cdot) \mid w_{-ij}(\cdot)$ for all $(i, j) \notin E$.

If C is a multivariate Matérn covariance function (Gneiting et al., 2010; Apanasovich et al., 2012), then each component $w_j(\cdot)$ of $w(\cdot) \sim GGP(C, \mathcal{G})$ is a Matérn GP. Hence, the spatial properties of each variable can be studied from the estimates of the respective Matérn covariance parameters. Construction of the graphical GP uses an algorithm called “stitching” which performs covariance selection using \mathcal{G} on C restricted to a finite set of locations \mathcal{L} , and then

extends it to the infinite domain. We first define covariance selection for positive definite (p.d.) matrices.

Definition 2.2. Given a graph $\mathcal{G} = (\mathcal{V}, E)$ and a matrix A with row and column blocks indexed by \mathcal{V} , $\text{CovSel}(A, \mathcal{G})$ is the unique p.d. matrix B from Dempster’s covariance selection on A using \mathcal{G} , i.e., $B_{ij} = A_{ij}$ for $i = j$ or $(i, j) \in E$, and $(B^{-1})_{ij} = 0$ for $(i, j) \notin E$.

Given C , \mathcal{G} and \mathcal{L} , stitching first defines the graphical GP on \mathcal{L} and then extends it to $\mathcal{D} \setminus \mathcal{L}$.

$$w_{\text{stitch}}(\mathcal{L}) \sim N(0, \tilde{C}(\mathcal{L}, \mathcal{L})) \text{ where } \tilde{C}(\mathcal{L}, \mathcal{L}) = \text{Covsel}(C(\mathcal{L}, \mathcal{L}), \mathcal{G}). \quad (1)$$

$$w_{\text{stitch},j}(s) = w_{\text{stitch},j}^{pp}(s) + z_j(s), \text{ where } w_{\text{stitch},j}^{pp}(s) = C_{jj}(s, \mathcal{L})C_{jj}(\mathcal{L}, \mathcal{L})^{-1}w_{\text{stitch},j}(\mathcal{L}) \quad (2)$$

is the low rank predictive process and $z_j(\cdot) \stackrel{\text{ind}}{\sim} GP(0, C_{jj, \text{res}})$ is the residual GP with $C_{jj, \text{res}}(s, t) = C_{jj}(s, t) - C_{jj}(s, \mathcal{L})C_{jj}(\mathcal{L}, \mathcal{L})^{-1}C_{jj}(\mathcal{L}, t)$. Decomposition of a univariate GP into a predictive process and an orthogonal residual process is well known (Banerjee et al., 2008). Stitching introduces two innovations to this decomposition. First, the process on \mathcal{L} is endowed with the covariance $\tilde{C}(\mathcal{L}, \mathcal{L})$ instead of $C(\mathcal{L}, \mathcal{L})$. This ensures that the graph is encoded while preserving marginals on \mathcal{L} . Orthogonality implies that the marginals are preserved over \mathcal{D} when the residual processes, $z_j(\cdot)$ ’s, are stitched to the low-rank Gaussian process $w_{\text{stitch},j}^{pp}(s)$. Second, the $z_j(\cdot)$ ’s are chosen to be component-wise independent ensuring that the graph encoded over \mathcal{L} is inherited to process-level conditional independence relations over \mathcal{D} .

For a decomposable sparse graph, stitched graphical GP likelihood involves considerably less parameters and FLOPs than that of a full GP with covariance C . Unlike functional GGM, stitched graphical GP does not require replicated data for parameter estimation or predictions.

3 Theoretical connections between functional GGM and graphical GP

3.1 Covariance selection on partially separable Gaussian processes

Consider a $q \times 1$ partially-separable multivariate GP on a continuous domain \mathcal{D} ,

$$w_0(s) = \sum_{l=1}^{\infty} \theta_l \phi_l(s), \text{ where } \theta_l = (\theta_{1l}, \dots, \theta_{ql}) \sim N_q(0, \Sigma_l). \quad (3)$$

Theorem 3.1 formally proves that the graphical GP derived from $w_0(\cdot)$ is a partially separable functional GGM that exactly preserves a given graphical model.

Theorem 3.1. *Let C be the cross-covariance function of a stationary partially separable process $w_0(\cdot)$ in (3). Consider a new partially separable process $w(s) = \sum_{l=1}^{\infty} \theta_l^* \phi_l(s)$ where $\theta_l^* = (\theta_{1l}^*, \dots, \theta_{ql}^*) \sim N_q(0, \Sigma_l^*)$. Then for any fixed graph $\mathcal{G} = (\mathcal{V}, E)$, $w(\cdot) \sim GGP(C, \mathcal{G})$ as in Definition 2.1 if and only if $\Sigma_l^* = \text{CovSel}(\Sigma_l, \mathcal{G})$ for all l .*

Proof. Denote $\Sigma_l = (\sigma_{lij})$, $\Sigma_l^* = (\sigma_{lij}^*)$, and $\Sigma_l^{*-1} = \Omega_l = (\omega_{lij}^*)$. The cross-covariance function of $w(\cdot)$ is denoted by $C^* = (C_{ij}^*)$ and the conditional cross-covariance function is $K^* = (K_{ij}^*)$. By Theorem 3 of Zapata et al. (2021),

$$K_{ij}^*(s, t) = \sum_{l=1}^{\infty} \frac{-\omega_{lij}^*}{\omega_{lil}^* \omega_{ljj}^* - \omega_{lij}^{*2}} \phi_l(s) \phi_l(t). \quad (4)$$

(If part:) Suppose $\Sigma_l^* = \text{CovSel}(\Sigma_l, \mathcal{G})$ for all l . To prove $w(\cdot) \sim GGP(C, \mathcal{G})$ we first show it is a graphical GP. For any $(i, j) \notin E$, by the property of covariance selection on each Σ_l , we have $\omega_{lij}^* = 0$ for all l . Hence, from (4) $K_{ij}^*(s, t) = 0$ for all $s, t \in \mathcal{D}$, $(i, j) \notin E$ and $w(\cdot)$ is a graphical GP with respect to the graph \mathcal{G} . Next we show $w(\cdot)$ retains the marginals and edge-specific cross-covariances from C . This is immediate as once again for all $(i, j) \ni i = j$ or $(i, j) \in E$, we have by the property of covariance selection $\sigma_{lij}^* = \sigma_{lij}$ and consequently $C_{ij}^*(s, t) = \sum_{l=1}^{\infty} \sigma_{lij}^* \phi_l(s) \phi_l(t) = \sum_{l=1}^{\infty} \sigma_{lij} \phi_l(s) \phi_l(t) = C_{ij}(s, t)$.

(Only if part:) Let $w(s) = \sum_{l=1}^{\infty} \theta_l^* \phi_l(s) \sim GGP(C, \mathcal{G})$. Since it is a graphical GP, then

$K_{ij}^*(s, t) = 0$ for all $s, t \in \mathcal{D}$ and $(i, j) \notin E$. By orthogonality of ϕ_l 's,

$$0 = \int K_{ij}^*(s, t) \phi_l(s) ds = \frac{-\omega_{lij}^*}{\omega_{lii}^* \omega_{ljj}^* - \omega_{lij}^{*2}} \phi_l(t).$$

This holds for all $t \in \mathcal{D}$ implying $\omega_{lij}^* = 0$ for all l . By definition (2.1), $w(\cdot)$ retains the marginal and edge-specific cross-covariances. Hence, for $i = j$ or $(i, j) \in E$, $C_{ij}^* = C_{ij}$ implying

$$\sigma_{lij} \phi_l(t) = \int C_{ij}(s, t) \phi_l(s) ds = \int C_{ij}^*(s, t) \phi_l(s) ds = \sigma_{lij}^* \phi_l(t).$$

This holds for all t implying $\sigma_{lij} = \sigma_{lij}^*$ for all $l, i = j$ or $((i, j) \in E)$. Hence, Σ_l^* satisfies all the conditions of covariance selection (Definition 2.2) and is the unique matrix $\text{CovSel}(\Sigma_l, \mathcal{G})$. \square

The result shows that starting with a partially separable GP, the graphical GP can be obtained by applying covariance selection on each covariance matrix of the basis coefficients, and this graphical GP is a partially separable functional GGM. We subsequently discuss in Section 4 how this facilitates an estimation strategy for functional GGM that exactly conforms to a given graph.

3.2 Stitching and truncation

In practice, we cannot work with infinite basis expansions and use a finite-term truncation. The following result on truncated functional GGM is an immediate consequence of Theorem 3.1.

Corollary 3.1.1. *Consider the truncated process $w_0^m(s) = \sum_{l=1}^m \theta_l \phi_l(s)$ with covariance function C^m . Then $w^m(\cdot) \sim GGP(C^m, \mathcal{G})$ is given by $w^m(s) = \sum_{l=1}^m \theta_l^* \phi_l(s)$ where $\text{Cov}(\theta_l^*) = \text{Covsel}(\Sigma_l, \mathcal{G})$ for $l = 1, \dots, m$.*

We now relate this truncated functional GGM $w^m(\cdot)$ to a low-rank stitched graphical GP (recall Section 2.2) through an approximate result. Let $w_0(\cdot)$ be the partially separable GP in (3) with cross-covariance function $C = (C_{ij})$, $w(\cdot)$ be the partially separable $GGP(C, \mathcal{G})$ derived from $w_0(\cdot)$ using Theorem 3.1 and $w^m(\cdot)$ be the finite-term truncation of $w(\cdot)$ in Corollary 3.1.1. Then $w^m(\cdot) \approx w_{stitch}^{pp}(\cdot)$, where $w_{stitch}^{pp} = (w_{stitch,1}^{pp}(\cdot), \dots, w_{stitch,q}^{pp}(\cdot))$ is the stitched predictive process defined in (2). To derive this result, we observe that $w_{stitch}^{pp}(s) = D(s)w_{stitch}(\mathcal{L})$ where

$D(s) = \text{diag}(C_{11}(s, \mathcal{L})C_{11}(\mathcal{L}, \mathcal{L})^{-1}, \dots, C_{qq}(s, \mathcal{L})C_{qq}(\mathcal{L}, \mathcal{L})^{-1})$ and $w_{\text{stitch}}(\mathcal{L})$ is a random variable whose distribution is specified in (1). Next, as $w(\cdot) \sim GGP(C, \mathcal{G})$, the component processes $w_j(\cdot) \sim GP(0, C_{jj})$ retain the marginals. When the reference set \mathcal{L} is chosen to have m locations, the truncated process $w_j^m(\cdot)$ will satisfy (see, e.g., p. 389-390 in Banerjee et al., 2014)

$$w_j^m(s) \approx C_{jj}(s, \mathcal{L})C_{jj}(\mathcal{L}, \mathcal{L})^{-1}w_j(\mathcal{L}) \text{ for all } s \in \mathcal{D}, j \in \mathcal{V}. \quad (5)$$

This approximate equivalence result is related the Nystrom approximation for kernel matrices (Drineas et al., 2005). Rewriting (5) as $w^m(s) \approx D(s)w(\mathcal{L})$ and since $w_{\text{stitch}}^{pp}(s) = D(s)w_{\text{stitch}}(\mathcal{L})$, we only need $w(\mathcal{L})$ and $w_{\text{stitch}}(\mathcal{L})$ to approximately have the same distribution to show $w^m(\cdot) \approx w_{\text{stitch}}^{pp}(\cdot)$. As $w(\cdot) \sim GGP(C, \mathcal{G})$, for $i = j$ or $(i, j) \in E$, we have $\text{Cov}(w_i(\mathcal{L}), w_j(\mathcal{L})) = C_{ij}(\mathcal{L}, \mathcal{L}) = \text{Cov}(w_{\text{stitch},i}(\mathcal{L}), w_{\text{stitch},j}(\mathcal{L}))$ by definition of covariance selection. Finally, we show that for $(i, j) \notin E$, $\text{Cov}(w_i(\mathcal{L}), w_j(\mathcal{L}) \mid w_{-(ij)}(\mathcal{L})) \approx O$ as follows:

$$\begin{aligned} \text{Cov}(w_i(\mathcal{L}), w_j(\mathcal{L}) \mid w_{-(ij)}(\mathcal{L})) &= \text{Cov}(C_{ii}(\mathcal{L}, \mathcal{L})C_{ii}(\mathcal{L}, \mathcal{L})^{-1}w_i(\mathcal{L}), \\ &\quad C_{jj}(\mathcal{L}, \mathcal{L})C_{jj}(\mathcal{L}, \mathcal{L})^{-1}w_j(\mathcal{L}) \mid C_{kk}(\mathcal{L}, \mathcal{L})C_{kk}(\mathcal{L}, \mathcal{L})^{-1}w_k(\mathcal{L}), k \in \mathcal{V} \setminus \{i, j\}) \\ &\approx \text{Cov}(w_i^m(\mathcal{L}), w_j^m(\mathcal{L}) \mid w_{-ij}(\mathcal{L})) \text{ by (5)} \\ &= \text{Cov}(w_i^m(\mathcal{L}), w_j^m(\mathcal{L}) \mid C_{kk}(s, \mathcal{L})C_{kk}(\mathcal{L}, \mathcal{L})^{-1}w_k(\mathcal{L}), s \in \mathcal{D}, k \neq i, j) \\ &\approx \text{Cov}(w_i^m(\mathcal{L}), w_j^m(\mathcal{L}) \mid w_{-ij}^m(\cdot)) \text{ again by (5)} \\ &= O \text{ for } (i, j) \notin E. \end{aligned}$$

The middle equality follows from the σ -algebras $\sigma(w_{-ij}(\mathcal{L}))$ and $\sigma(C_{kk}(s, \mathcal{L})C_{kk}(\mathcal{L}, \mathcal{L})^{-1}w_k(\mathcal{L}), s \in \mathcal{D}, k \neq i, j)$ being the same since the latter is generated by the former and contains the former. Corollary 3.1.1 ensures the last equality since $w^m(\cdot)$ is a graphical GP conforming to \mathcal{G} .

This establishes the equivalence of m -truncated partially separable GP with a stitched low-rank predictive process on m reference locations. Analogous to Theorem 3.1, proving the equivalence of the theoretical constructions of functional GGM and graphical GP, this result establishes an analogy between the practical procedures of truncation and stitching for the two approaches. Section 3.2 also highlights an important distinction between truncation and

stitching. Stitched graphical GPs, as specified in (2), is the sum of a stitched low-rank predictive process and an independent residual processes, $w_{stitch}(s) = w_{stitch}^{pp}(s) + z(s)$, where $z(s) = (z_1(s), \dots, z_q(s))$. The truncated functional GGM is only equivalent to the first component and ignores the residual component; i.e., $w_{stitch}(s) \approx w^m(s) + z(s)$. This is a potential drawback of the truncated functional GGM as it does not respect the marginals and edge-specific cross-covariances of the original process. To see this, we state with the following.

Theorem 3.2. *Let $w_0^{pp}(\cdot) \sim GP(0, C^{pp})$ denote the finite-rank predictive process approximation of $w_0(\cdot)$ on \mathcal{L} (Banerjee et al., 2008), i.e., $w_0^{pp}(s) = D(s)w_0(\mathcal{L})$. Then the stitched predictive process $w_{stitch}^{pp}(s) = D(s)w_{stitch}(\mathcal{L})$ of (2) is $GGP(C^{pp}, \mathcal{G})$.*

Proof. As $w_0(\mathcal{L})$ and $w_{stitch}(\mathcal{L})$ agree on the marginals and edge-specific cross-covariances, so do $w_0^{pp}(s) = D(s)w_0(\mathcal{L})$ and $w_{stitch}^{pp}(s) = D(s)w_{stitch}(\mathcal{L})$. Also, as $\{D(s)w_{stitch}(\mathcal{L}) : s \in \mathcal{D}\}$ is generated by $w_{stitch}(\mathcal{L})$ and contains $w_{stitch}(\mathcal{L})$, the sigma algebras $\sigma(\{D(s)w_{stitch}(\mathcal{L}) : s \in \mathcal{D}\})$ and $\sigma(w_{stitch}(\mathcal{L}))$ are the same. Since $w_{stitch}(\mathcal{L})$ is a GGM on \mathcal{L} , $D(s)w_{stitch}(\mathcal{L})$ is a graphical GP on \mathcal{D} with respect to \mathcal{G} proving $w_{stitch}^{pp} = D(s)w_{stitch}(\mathcal{L}) \sim GGP(C^{pp}, \mathcal{G})$. \square

The multivariate predictive process $w_0^{pp}(\cdot)$ has been shown, theoretically and empirically, to underestimate the marginal variances of the original process $w_0(\cdot)$, oversmoothing and inferior performance (Stein, 2014; Datta et al., 2016). From Theorem 3.2, we know that the stitched predictive process $w_{stitch}^{pp}(\cdot)$ is the graphical GP that preserves the marginals from the multivariate predictive process w_0^{pp} . Hence, $w_{stitch}^{pp}(\cdot)$ inherits these issues of not retaining the marginals of the original process and so will the truncated functional GGM $w^m(\cdot)$ (using the approximate equivalence between the two shown in this Section). For a univariate predictive process this deficiency is fixed by adding the residual process (Finley et al., 2009). Stitching proceeds similarly in a multivariate graphical model by introducing $z(\cdot)$ in (2) to exactly preserve the marginals. Next, we leverage this connection between truncation and stitching to present an estimation strategy for functional GGM that allows conducting multivariate functional analysis while preserving both the graph and the marginals.

4 Estimation

In scientific applications, we either know the graph apriori or have to estimate it. Functional GGM is widely deployed in the former setting (Zapata et al., 2021; Krock et al., 2021). However, if the graph is known (e.g., a known phylogenetic tree as a graph to model multiple species distributions over a region or a known auto-regressive time-dependence structure to model spatio-temporal pollutant data), current functional GGM approaches cannot explicitly encode this information and preserve the graphical model in the analysis.

Theorem 3.1 enables an extension of partially separable functional GGM that conforms to a given graph. Under the constraint of a given graphical model \mathcal{G} , we want to find the maximum likelihood estimate (MLE) of the covariance operator C of random multivariate functional observations X_1, \dots, X_N generated from a mean-zero partial separable GP $w_0(s)$ as in (3). Let $\Sigma_l = \text{diag}(\sqrt{\sigma_l})R_l\text{diag}(\sqrt{\sigma_l})$ where R_l denotes the correlation matrix for θ_l . Let \hat{R}_l denote the MLE of R_l without any graphical constraints and $M^+(\mathcal{G}) = \{S \in \mathbb{R}^{q \times q} : S_{ij} = 0 \forall (i, j) \notin E\}$, then following Dempster (1972) the MLE of R_l that respects \mathcal{G} is given by

$$\left(\underset{\Gamma_l \succ 0, \Gamma_l \in M^+(\mathcal{G}_V)}{\text{argmin}} [\text{tr}(\hat{R}_l \Gamma_l) - \log(|\Gamma_l|)] \right)^{-1} = \text{CovSel}(\hat{R}_l, \mathcal{G}), \quad (6)$$

From Theorem 3.1 and Corollary 3.1.1, the MLE for C that conforms to \mathcal{G} is obtained as

$$\hat{C} = \sum_{l=1}^m (\text{diag}(\sqrt{\hat{\sigma}_l})^\top \text{CovSel}(\hat{R}_l, \mathcal{G}) \text{diag}(\sqrt{\hat{\sigma}_l})) \hat{\phi}_l \otimes \hat{\phi}_l \quad (7)$$

Here, following Zapata et al. (2021), the basis functions estimates $\hat{\phi}_l$ are from a functional principal components analysis. We formally lay out the above steps in Algorithm 1 in the Supplement and term our approach as FGGM-CovSel.

The truncation m is usually chosen so that the first m eigen-functions $\hat{\phi}_l$'s explain a given percentage ν of the total variance. A larger ν improves the retention of marginal covariance functions but requires larger m . Covariance selection on the R_l 's is performed using the iterative proportional scaling (IPS) algorithm (Speed et al., 1986) which has a total complexity of $O(mq^3)$ FLOPs for the m terms. For large q , this mandates choosing a smaller m to reduce

computations. This tradeoff leads to a worse approximation of the marginal covariances as finite-term truncation is equivalent to low-rank stitching at m locations (see the discussion in Section 3.2).

To remedy this, we modify Algorithm 1 to emulate the full rank stitching procedure of Dey et al. (2021) by adding component specific residual processes. We first run FGGM-CovSel for a small or moderate m as afforded by the computing resources. Then, we calculate the residuals and perform functional principal component analysis of the component-specific residuals and add the diagonal matrix of the estimated residual variances to our covariance estimate \hat{C} from Algorithm 1. Adding residual terms to the truncated functional GGM independently for each component process is equivalent to constructing the full-rank stitched graphical GP in (2) by adding the independent z_j 's to the stitched predictive process $w_{stitch,pp}$. This yields significant improvements in retaining the univariate distributions. The Algorithm is referred to as FGGM-Stitch and is formally laid out in Algorithm 2 of the Supplement.

5 Simulation studies

We perform a series of simulation experiments to gauge the performance accuracy of FGGM, FGGM-CovSel and FGGM-Stitch algorithms. The details of the data-generation mechanisms are provided in Section S2 of the Supplement. In Figure 1 we compare the true and estimated marginal covariance functions for a correctly specified setting for the FGGM. We see that FGGM-Stitch has a significantly improved estimate of the marginal covariance than both FGGM and FGGM-CovSel. This aligns with our theoretical insights from Section 3.2. For the cross-covariances, FGGM-Stitch and FGGM-CovSel estimates are the same. From Figure S2 we see that they offer improvement over the FGGM estimate on account of exactly preserving the graph. This improvement is consistent across all the edge-specific cross-covariances and also in misspecified settings (Table S1). We refer to Section S2 for more details on the results.

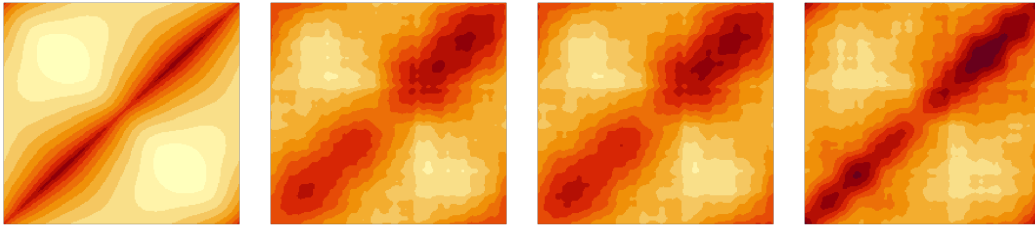


Figure 1: *Marginal covariance surfaces for variable 1: True, FGGM, FGGM-CovSel, FGGM-Stitch (from left to right).*

References

- APANASOVICH, T. V., GENTON, M. G. & SUN, Y. (2012). A valid matern class of cross-covariance functions for multivariate random fields with any number of components. *Journal of the American Statistical Association* **107**, 180–193.
- BANERJEE, S., CARLIN, B. P. & GELFAND, A. E. (2014). *Hierarchical modeling and analysis for spatial data*. Chapman and Hall/CRC.
- BANERJEE, S., GELFAND, A. E., FINLEY, A. O. & SANG, H. (2008). Gaussian predictive process models for large spatial data sets. *Journal of the Royal Statistical Society: Series B (Statistical Methodology)* **70**, 825–848.
- CARVALHO, C. M., MASSAM, H. & WEST, M. (2007). Simulation of hyper-inverse wishart distributions in graphical models. *Biometrika* **94**, 647–659.
- CRESSIE, N. A. C. & WIKLE, C. K. (2011). *Statistics for spatio-temporal data*. Wiley Series in Probability and Statistics. Hoboken, NJ: Wiley.
- DATTA, A., BANERJEE, S., FINLEY, A. O. & GELFAND, A. E. (2016). Hierarchical nearest-neighbor Gaussian process models for large geostatistical datasets. *Journal of the American Statistical Association* **111**, 800–812.
- DEMPSTER, A. P. (1972). Covariance selection. *Biometrics* , 157–175.
- DEY, D., DATTA, A. & BANERJEE, S. (2021). Graphical Gaussian Process Models for Highly Multivariate Spatial Data. *Biometrika* Asab061.

- DOBRA, A., LENKOSKI, A. & RODRIGUEZ, A. (2011). Bayesian inference for general gaussian graphical models with application to multivariate lattice data. *Journal of the American Statistical Association* **106**, 1418–1433.
- DRINEAS, P., MAHONEY, M. W. & CRISTIANINI, N. (2005). On the nyström method for approximating a gram matrix for improved kernel-based learning. *journal of machine learning research* **6**.
- FINLEY, A. O., SANG, H., BANERJEE, S. & GELFAND, A. E. (2009). Improving the performance of predictive process modeling for large datasets. *Computational statistics & data analysis* **53**, 2873–2884.
- FRIEDMAN, J., HASTIE, T. & TIBSHIRANI, R. (2008). Sparse inverse covariance estimation with the graphical lasso. *Biostatistics* **9**, 432–441.
- GNEITING, T., KLEIBER, W. & SCHLATHER, M. (2010). Matérn cross-covariance functions for multivariate random fields. *Journal of the American Statistical Association* **105**, 1167–1177.
- KROCK, M., KLEIBER, W., HAMMERLING, D. & BECKER, S. (2021). Modeling massive highly-multivariate nonstationary spatial data with the basis graphical lasso. *arXiv preprint arXiv:2101.02404* .
- MEINSHAUSEN, N. & BÜHLMANN, P. (2006). High-dimensional graphs and variable selection with the lasso. *The annals of statistics* **34**, 1436–1462.
- OH, S.-Y. & PETERSEN, A. (2019). *fgm: Partial Separability and Functional Gaussian Graphical Models*. R package version 1.0.
- PENG, J., WANG, P., ZHOU, N. & ZHU, J. (2009). Partial correlation estimation by joint sparse regression models. *Journal of the American Statistical Association* **104**, 735–746.
- QIAO, X., GUO, S. & JAMES, G. M. (2019). Functional graphical models. *Journal of the American Statistical Association* **114**, 211–222.

- ROVERATO, A. (2002). Hyper inverse wishart distribution for non-decomposable graphs and its application to bayesian inference for gaussian graphical models. *Scandinavian Journal of Statistics* **29**, 391–411.
- SPEED, T. P., KIIVERI, H. T. et al. (1986). Gaussian markov distributions over finite graphs. *The Annals of Statistics* **14**, 138–150.
- STEIN, M. L. (1999). Interpolation of spatial data: some theory for kriging .
- STEIN, M. L. (2014). Limitations on low rank approximations for covariance matrices of spatial data. *Spatial Statistics* **8**, 1–19.
- WACKERNAGEL, H. (2013). *Multivariate geostatistics: an introduction with applications*. Springer Science & Business Media.
- YANG, W., MÜLLER, H.-G. & STADTMÜLLER, U. (2011). Functional singular component analysis. *Journal of the Royal Statistical Society: Series B (Statistical Methodology)* **73**, 303–324.
- YAO, F., MÜLLER, H.-G. & WANG, J.-L. (2005). Functional data analysis for sparse longitudinal data. *Journal of the American statistical association* **100**, 577–590.
- ZAPATA, J., OH, S. Y. & PETERSEN, A. (2021). Partial separability and functional graphical models for multivariate Gaussian processes. *Biometrika* Asab046.
- ZHU, H., STRAWN, N. & DUNSON, D. B. (2016). Bayesian graphical models for multivariate functional data .

Supplementary Materials for “On the Relationship between Graphical Gaussian Processes and Functional Gaussian Graphical Models”

Debangana Dey, Abhirup Datta, Sudipto Banerjee

S1 Algorithms for Section 5

Algorithm 1. (FGGM-CovSel)

1. Fix a proportion of variance explained threshold, v , say, $v = 0.95$;
2. Perform pooled functional principal component analysis (Yao et al. (2005); Yang et al. (2011)) to get m common eigenfunction estimates $\hat{\phi}_l, l = 1, \dots, m$ that explain v proportion of total variance. ;
3. Use the eigenfunctions to get first m functional principal component scores $\hat{\theta}_l$ and calculate the corresponding correlation matrix $\hat{R}_l = \text{cor}(\hat{\theta}_l)$ for $l = 1, \dots, m$;
4. Using Iterative Proportional Scaling (IPS) algorithm (Speed et al., 1986) for covariance selection, obtain the estimates of the precision matrices $\text{CovSel}(\hat{R}_l, \mathcal{G})$ for $l = 1, \dots, m$;
5. We obtain the estimate of the covariance operator \hat{C} from (7).

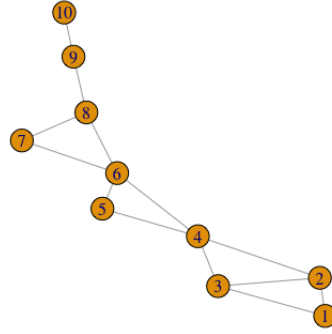
Algorithm 2. (FGGM-Stitch)

1. Fix a smaller proportion of variance explained threshold, v , say, $v = 0.75$;
2. Run Algorithm 1 to get estimates $\hat{\theta}_l, \hat{\phi}_l, l = 1, \dots, m$ and \hat{C} ;
3. Calculate residuals: $Z_i = X_i - \sum_{l=1}^m \hat{\theta}_l \hat{\phi}_l$ for $i = 1, \dots, N$;
4. Perform functional principal component analysis of the residuals of $Z^{(j)} = (Z_{1j}, \dots, Z_{Nj})$ for $j = 1, \dots, q$ independently for a larger proportion of variance explained, v' , say, $v' = 0.95$;
5. Obtain the eigenvalues as $\hat{\lambda}_{lj}, l = 1, \dots, m', j = 1, \dots, q$;
6. Find the new stitched covariance operator $\hat{C}^{(2)} = \hat{C} + \sum_{l=1}^{m'} \text{diag}(\hat{\lambda}_{l1}, \dots, \hat{\lambda}_{lq})$.

S2 Detailed Simulation Results

For the data-generation in the simulation studies, we consider $q = 10$ variable GPs obeying the conditional independence structure from the graph in Figure S1. We consider two data-generating mechanisms – (a) PS: Partial-separable GP of (Zapata et al., 2021) – We fix total number of basis functions at $L = 101$ for data generation. We take them to be the Fourier basis functions and evaluate them at 200 equally spaced points between $(0, 1)$. Now to generate the basis-specific coefficients, we generate the covariance matrices as $\Sigma_l = a_l \Omega_l^{-1}$ for $l = 1, \dots, 101$, where, the precision matrices Ω_l are generated for the graph \mathcal{G} (Figure S1) based on the algorithm of Peng et al. (2009). The decaying constants $a_l = 3l^{-1.8}$ ensure that $\text{tr}(\Sigma_l)$ is monotonically decreasing in l . (b) GM: Graphical Matérn of (Dey et al., 2021) – The cross-covariance functions were obtained by stitching (Dey et al., 2021) using multivariate Matérn model (Apanasovich et al., 2012) and the graph \mathcal{G} (Figure S1). For every (i, j) pair of variables, the isotropic multivariate Matérn cross-covariance function on a d -dimensional domain is defined as $C_{ij}(s, s') = \sigma_{ij} H_{ij}(\|s - s'\|)$, where $H_{ij}(\cdot) = H(\cdot | \nu_{ij}, \phi_{ij})$, H being the Matérn correlation function (Apanasovich et al., 2012). $\sigma_{ij}, \phi_{ij}, \nu_{ij}$ are interpreted as the cross-covariance, cross-scale and cross-smoothness parameters. To ensure positive-definiteness of cross-covariance matrix, we parametrize as $\sigma_{ij} = b_{ij} \frac{\Gamma(\frac{1}{2}(\nu_{ii} + \nu_{jj} + d)) \Gamma(\nu_{ij})}{\phi_{ij}^{2\Delta_A + \nu_{ii} + \nu_{jj}} \Gamma(\nu_{ij} + \frac{d}{2})}$, where $b_{ij} = (\sigma_{ii} \sigma_{jj})^{\frac{1}{2}} \phi_{ii}^{\nu_{ii}} \phi_{jj}^{\nu_{jj}} \frac{r_{ij}}{\Gamma(\nu_{ij})}$, and $R = (r_{ij}) > 0$, is correlation matrix. For this simulation, we take $\nu_{ij} = \nu_{ii} = \nu_{jj} = \frac{1}{2}$, and $\Delta_A = 0$ and $\phi_{ij}^2 = (\phi_{ii}^2 + \phi_{jj}^2)/2$. The marginal range parameters ϕ_{ii} and variance parameters σ_{ii} were permutations of equispaced numbers in $(1, 5)$, while the $R = r_{ij}$'s were chosen as a random correlation matrix. For data generation locations, we take 250 points on the real line equispaced between $(0, 1)$.

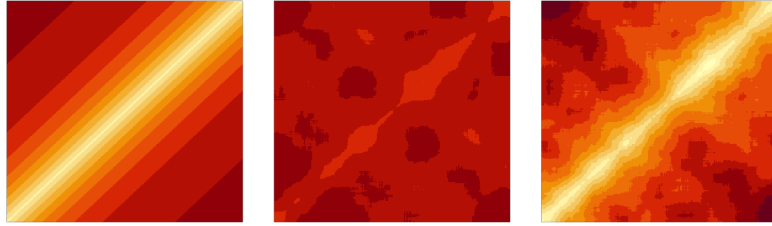
Figure S1: The 10-variable graph for simulation



We compare the estimated marginal and edge-specific cross-covariance surfaces qualitatively using some heat-maps and quantitatively using the distance between true and estimated covariance sub-matrices in terms of Kullback-Leibler (KL) divergence. The KL divergence between two matrices A and B is defined as- $\text{KL}(B \parallel A) = \frac{1}{2}(\text{tr}(A^{-1}B) - \log(\frac{|A|}{|B|}))$. In case (a), which is the truly specified case, we present the results comparing FGGM-CovSel and the FGGM algorithm in Zapata et al. (2021) (implemented using the R package *FGM* (Oh & Petersen, 2019)). The estimates of the cross-covariance surfaces for the proposed algorithms FGGM-CovSel and FGGM-Stitch are the same. This estimate performs better than the FGGM estimate (Figure S2a). This behavior is expected since FGGM assumes the graph structure as unknown. Case (b) presents a mis-specified scenario where the data is generated from a non-partial separable multivariate GP such as Graphical Matérn. Figure S2b shows that FGGM-CovSel performs poorer than the Set (a) but captures the banded patterns of Matérn to some extent. This difficulty is expected since we're trying to fit a misspecified partial separable cross-covariance to a non-partially separable GP. Overall, across all edges (Table S1) and in both simulation scenarios, FGGM-CovSel reports lower KL divergence between true and estimated matrices than FGGM. FGGM-CovSel performs according to our expectations in both of the examples thus validating the theoretical basis of our approach. This is in addition to the benefit demonstrated in Figure 1 of using FGGM-Stitch to better capture the marginal variances.



(a) Set (a): The estimated cross-covariance surface of (1, 2) edge: True, FGGM, FGGM-CovSel (from left to right)



(b) Set (b): The estimated cross-covariance surface of (1, 2) edge: True, FGGM, FGGM-CovSel (from left to right)

Figure S2: Comparison of (1, 2) variable pair cross-covariance surface heatmaps under different simulation scenarios

		Set (a)		Set (b)	
Edges		FGGM	FGGM-CovSel	FGGM	FGGM-CovSel
1	(1, 2)	772.33	730.14	1756.63	1743.67
2	(1, 3)	781.86	778.54	1968.73	1947.28
3	(2, 3)	765.56	745.51	1857.85	1849.48
4	(2, 4)	759.82	737.58	1750.40	1745.11
5	(3, 4)	789.61	771.73	1963.20	1954.73
6	(4, 5)	758.68	735.18	1881.67	1871.14
7	(4, 6)	794.68	779.10	1870.62	1828.11
8	(5, 6)	739.91	736.03	1886.16	1875.10
9	(6, 7)	799.06	759.31	1951.70	1933.22
10	(6, 8)	822.02	796.03	1318.02	1293.61
11	(7, 8)	795.01	776.45	1352.17	1341.08
12	(8, 9)	776.40	771.57	1088.51	1073.05
13	(9, 10)	776.98	743.57	1818.09	1796.54

Table S1: The KL divergence between true and estimated cross-covariance matrices (through FGGM and FGGM-CovSel) corresponding to all edges for Simulation sets (a) and (b)